Wang *et al. Energy Mater* 2024;4:400031
DOI: 10.20517/energymater.2023.103

Energy Materials

Article

Open Access

Check for updates

Porous array of $BaLi_4$ alloy microchannels enforced carbon cloth for a stable Li composite anode

Zihao Wang[1,3], Tao Chen[2], Zhicui Song[1,3], Jianxiong Xing[1,3], Aijun Zhou[1,3], Jingze Li[1,3,*]

[1]School of Materials and Energy, University of Electronic Science and Technology of China, Chengdu 611731, Sichuan, China.
[2]School of Electronic Engineering, Chengdu Technological University, Chengdu 611730, Sichuan, China.
[3]Huzhou Key Laboratory of Smart and Clean Energy, Yangtze Delta Region Institute (Huzhou), University of Electronic Science and Technology of China, Huzhou 313001, Zhejiang, China.

***Correspondence to:** Prof. Jingze Li, School of Materials and Energy, University of Electronic Science and Technology of China, No. 4, Section 2, Jianshe North Road, Chenghua District, Chengdu 611731, Sichuan, China. E-mail: lijingze@uestc.edu.cn

How to cite this article: Wang Z, Chen T, Song Z, Xing J, Zhou A, Li J. Porous array of $BaLi_4$ alloy microchannels enforced carbon cloth for a stable Li composite anode. *Energy Mater* 2024;4:400031. https://dx.doi.org/10.20517/energymater.2023.103

Received: 12 Dec 2023 **First Decision:** 21 Feb 2024 **Revised:** 12 Mar 2024 **Accepted:** 27 Mar 2024 **Published:** 9 Apr 2024

Academic Editors: Hong Xu, Cheol-min Park **Copy Editor:** Fangling Lan **Production Editor:** Fangling Lan

Abstract

Integrating metallic lithium (Li) with a three-dimensional (3D) host is a popular strategy for long-life Li composite anodes, where the structure and physicochemical nature of the framework are critical for the electrochemical performance. Herein, Li-rich dual-phase barium (Ba)-based alloy composed of $BaLi_4$ intermetallic compounds and Li metal phases is thermally incorporated into commercial carbon cloth sheets to develop Li-Ba alloy composite (LBAC) anodes featuring a porous array of $BaLi_4$ microchannels as the built-in 3D skeleton. Doping of metallic Ba can greatly lower the surface tension of liquid Li and improve the wettability of the molten Li-Ba alloy toward the carbon cloth substrate. Moreover, LBAC benefits from the superior lithiophilicity and the porous architecture of $BaLi_4$ skeleton nested in a conductive carbon fiber matrix, leading to stable cycling performance by confining Li stripping/plating in microchannels network of $BaLi_4$ alloy framework and dissipating high current densities. As a result, the LBAC symmetrical cells can run stably for 1,000 h under 1 mA cm^{-2} and 1 mA h cm^{-2}, and the capacity retention can retain 93.3% after 300 cycles in the full cell with areal capacity of 2.45 mA h cm^{-2}. This work offers a smart designing strategy of 3D Li alloy composite anodes by introducing porous and lithiophilic alloy scaffold as sub-framework of the carbon hosting anode, promising the prospect of Li metal batteries for future applications.

Keywords: Li composite anode, carbon cloth, Li-Ba alloy, wettability, microchannels

INTRODUCTION

Lithium (Li) metal has high specific capacity (3,860 mA h g^{-1}) and the lowest electrochemical potential (-3.04 V *vs.* standard hydrogen electrodes), which is considered to be a potential choice for high energy density Li-based batteries[1-4]. However, the commercialization of Li metal batteries is severely limited by the volume variation associated with the "hostless" bare Li anode and the uncontrolled Li dendrite growth. Generally, hosting Li with the three-dimensional (3D) framework has been regarded as a popular method to improve the lifespan of Li anodes[5-11]. To encapsulate Li metal in a 3D framework, thermal infusion strategies involving introducing molten Li into a 3D matrix have been developed[12-18]. Among various 3D hosts, carbon-based frameworks are recognized to be an ideal host architecture due to their lightweight, high mechanical strength, excellent electrical conductivity, low-cost, and abundance in nature[19-26]. For instance, Wang *et al.* proposed that molten Li can be easily impregnated into carbon nanotube (CNT) network to form Li-CNT composites, which not only exhibit high specific capacity but also suppress Li dendrite formation[27].

Remarkably, the liquid Li has high surface tension and the poor lithiophilicity of carbon materials causes the liquid Li to display a spherical shape on the most carbon-based substrates, indicating the molten Li is difficult to diffuse into the interior of the carbon-based skeleton, which poses an obstacle for the fabrication of Li composite anodes[28-31]. Therefore, further modification of carbon-based hosts is required to tune the wettability. Apparently, the binding energy among Li atoms can be reduced by some substances that can react with Li metal to form Li compounds or alloys, thus decreasing the surface tension of molten Li and improving the wettability[32]. Coating lithiophilic layers have been widely employed to decorate the carbon-based framework[33-40]. For example, Zhu *et al.* reported a carbon scroll, which consists of vertically aligned carbon fibers decorated with copper oxide (CuO_x) nanoparticles[33]. The CuO_x can react with metallic Li to produce Cu and Li_2O chemically, which facilitates the wettability of liquid Li to carbon scroll, thus enabling Li metal to be well accommodated inside the skeleton. Alternatively, Wang *et al.* coated carbon cloth (CC) with ZnO nanoarray to obtain 3D porous hosts[41]. Molten Li can be infiltrated into such a 3D host rapidly due to the enhanced wettability of liquid Li toward 3D porous CC@ZnO. Notably, the nano-scale ZnO coating not only offers the driving force for wettability but also enables the formation of a Li-Zn alloy, exhibiting an exceptionally high Li^+ diffusion coefficient and facilitating the uniform Li deposition. However, the Li_2O *in situ* deduced from metal oxide layers can increase the interfacial impedance and prevent the substrate from being perfectly wetted by the molten Li[28]. To avoid this shortcoming, the non-metallic or metallic species that can react with liquid Li to produce Li_2O-free Li alloy have been investigated[42-45]. Zhang *et al.* introduced Si nanowire arrays on commercial CC sheets to fabricate a lithiophilic host[42]. The Si nanowires enhanced the wettability due to the generation of $Li_{22}Si_5$. The same phenomenon is repeated by Ag-coated framework. Zhang *et al.* found that Ag nanoparticles react with Li to produce Li-Ag alloy, which shows favorable Li affinity[45]. In addition, Ag nanoparticles can also act as the lithiophilic sites, promoting the Li nucleation process uniformly. On the other hand, regulating the micro/nanostructure on the surface of the carbon-derived substrate is also a promising strategy to improve the wettability[46-51]. Feng *et al.* introduced inactive transition metal nanoparticles (Ni, Cu) onto the surface of CC sheets to form capillary-like structure with conical gaps[47]. When the modified CC was in contact with liquid Li, the generated Laplace pressure forced the molten Li to diffuse into the CC at 220 °C, thereby significantly improving the wettability. It should be pointed out that the radial length of these lithiophilic architectures anchored on carbon-based substrate is only a few micrometers, which has relatively low specific area and is susceptible to being buried by the deposited Li, especially under a high Li plating capacity. This indicates that the conventional host has a limited ability to promote the Li stripping/plating behavior, and Li dendrites will grow uncontrollably on the electrode surface after multiple cycles[38,52]. Therefore, it is essential to design a continuous network of the lithiophilic species with the micro/nano-scale

pores as the sub-skeleton, which can not only confine the Li deposition/dissolution behavior in the limited space but also tackle the wettability issue of the carbon-based primary framework, leading to the improved performance of Li composite anodes.

Recently, it has been shown that generating Li-rich Li-X (where X denotes metallic element) alloy by doping other metals into liquid Li can significantly facilitate rapid spreading of molten Li by reducing surface tension[53-55]. In addition, the formed Li alloy phase can act as a 3D framework to regulate Li stripping/plating process for prolonged cyclic lifetime. The geometric structure and physicochemical nature of the Li alloy framework are critical for advanced performance of Li composite anodes. Our group found that dual-phase Li-barium (Ba) alloy has a unique micro-sized ordered array of $BaLi_4$ microchannels, which can homogenize Li^+ flux and provide active sites for inducing the uniform Li deposition[56]. However, the long-term cyclic stability cannot be guaranteed due to the insufficient robustness of the Li-Ba alloy scaffold.

Herein, we infiltrate the molten Li-rich Li-Ba alloy composed of $BaLi_4$ intermetallic compounds and Li metal phases into the CC sheet to fabricate a Li-Ba alloy composite anode (named LBAC). Doping of metallic Ba can significantly lower the binding force among Li atoms, allowing the molten liquid alloy to diffuse rapidly into the CC host. In addition, the $BaLi_4$ alloy scaffold is *in situ* created by phase separation during the cooling process. The porous architecture of $BaLi_4$ skeleton with strong lithiophilicity is nested in conductive carbon fiber network as the sub-framework, which provides larger surface area for the nucleation of Li and confines Li stripping/plating in microchannels of $BaLi_4$ alloy framework, thus suppressing the Li dendrite growth efficiently. Moreover, the structural stability of the Li-Ba alloy is enhanced by the strong flexibility exhibited by the CC. As a result, the LBAC anode displays favorable cycling performance, achieving ultra-long cycle lifespan (> 1,000 h) at 1 mA cm^{-2} and 1 mA h cm^{-2} in a symmetric cell with carbonate-based electrolyte. The LBAC/$LiFePO_4$ (LFP) full cell also displays outstanding long-term cycling lifespan and rate performance.

EXPERIMENTAL

Fabrication of LBAC electrode

The stainless steel (SS) foil was utilized as a substrate for the combination of metallic Li (99.5%, Chengdu Denway Newtype Metal Material Co., Ltd) and Ba (99.5%, Aladdin), with a molar ratio of 1:25. Then, the temperature was raised to 400 °C. A circular CC sheet measuring 12 mm in diameter was placed on the molten Li-Ba alloy after the complete dissolution of metallic Ba into liquid Li. The liquid Li-Ba alloy was quickly infiltrated into the CC sheet. Finally, the LBAC electrode was fabricated via a quick cooling treatment. All the operations were performed in an argon-filled glove box (Mikrouna, O_2 < 0.01 ppm, H_2O < 0.01 ppm). As a reference, except that the temperature was 500 °C, the Li-C anode was prepared by infiltrating the molten Li into the CC sheet.

Materials characterization

The LBAC anode and CC were recorded by X-ray diffraction (XRD) from 10 to 90° at 5° min^{-1} (Cu Kα, 0.15456 nm). The anode morphology was characterized using field emission scanning electron microscopy (FE-SEM) with an acceleration voltage of 20 kV.

Electrochemical measurements

The CR2032-type coin cells were utilized for the assembly of all cells, which were subsequently subjected to testing on a CT2001A battery testing system (LAND Electronic Co. Ltd.) at 25 °C. The working electrodes of symmetrical cells were LBAC, Li-C, or Li-Ba sheets. To standardize, symmetric cells were prepared using an electrolyte containing 100 μL of $LiPF_6$ (1 M) dissolved in a mixture of ethylene carbonate and diethyl carbonate (EC/DEC, v:v = 1:1), supplemented with 5% fluoroethylene carbonate (FEC). As a separator,

Celgard 2325 membranes were used. A CHI660C electrochemical workstation (Shanghai, Chenhua) measured electrochemical impedance spectra (EIS) in a frequency range of 0.1 Hz to 1 MHz.

Full cells were assembled using LFP cathodes, a Celgard 2325 separator, and a Li composite anode (Li-C, Li-Ba or LBAC anodes). As for LFP electrodes, a slurry of LFP powders, a super P conducting additive, and a binder made of polyvinylidene fluoride (PVDF) was fabricated by mixing them together in N-methyl-2-pyrrolidone (NMP) with a weight ratio of 8:1:1. The areal capacity of LFP electrodes was about 2.45 mA h cm^{-2}. The voltage range for measuring the full cells based on LFP was set between 2.2 and 3.85 V.

RESULTS AND DISCUSSION

The LBAC electrode is obtained by contacting CC disk with molten Li-Ba alloy. As shown in Figure 1A, when the CC touches the liquid Li-Ba alloy, the silver-white molten Li-Ba alloy can fill up the entire CC in less than 10 s, indicating that doping of metallic Ba can significantly lower the surface tension of liquid Li and improve the wettability toward CC. Based on the phase diagram of Li-Ba [Supplementary Figure 1], we can observe that phase segregated Li-Ba dual-phase alloy is composed of $BaLi_4$ intermetallic compounds and Li metal when the Li atomic percentage is larger than 80% and the temperature is lower than 143 °C. Thus, phase separation occurs when the temperature cools rapidly below 143 °C. On the contrary, the CC itself exhibits poor wettability towards liquid Li, so the Li metal does not diffuse into the CC in more than 60 s under the same conditions [Supplementary Figure 2A]. Notably, molten Li-Ba alloy exhibits more favorable wettability than other Li alloys (such as Li-Ca and Li-Ag)[57], which is one of the important merits considering the practical application. The top surface of LBAC is dark gray with the distinct textile pattern of the carbon fibers. As depicted in the top-view scanning electron microscopy (SEM) images [Figure 1B-D], the Li-Ba alloy fills the gaps between each bundle of carbon fibers. The phase segregation behavior in the cooling process forces the $BaLi_4$ phase to condense into a porous architecture with a relatively small diameter of about 20 μm. Apparently, the $BaLi_4$ sub-skeleton in LBAC can further increase the specific surface area of CC, providing a lower local current density and abundant sites of Li nucleation significantly. Meanwhile, the pores of the $BaLi_4$ alloy scaffold were filled with metallic Li, suggesting that the porous framework of the $BaLi_4$ network can host Li [Figure 1E-G]. Moreover, the pores of the $BaLi_4$ alloy scaffold are filled with metallic Li completely, indicating no voids in the as-prepared LBAC anodes. By deep contrast, as for the Li-C composite shown in Supplementary Figure 2B and C, the metallic Li almost covers the skeleton surface of the CC, and the void spaces among carbon fibers have been occupied by Li metal. From the side-view morphology of Li-C anodes [Supplementary Figure 2D and E], the metallic Li is not tightly bonded to the carbon fibers. The *ex-situ* XRD test was performed for confirming the composition of LBAC. As depicted in Supplementary Figure 3, the primary diffraction peaks of LBAC originate from the metallic Li phase, $BaLi_4$ and carbon. In Supplementary Table 1, the mass of Li in the LBAC anode is 16.2 mg with a weight percentage of ~42.1%. Additionally, LBAC exhibits a remarkable specific capacity of ~1,519 mAh g^{-1} after stripping Li to 2 V [Supplementary Figure 4], which closely approaches the theoretical specific capacity (1,621 mA h g^{-1}).

The Li stripping/plating behaviors of LBAC were conducted by SEM so as to analyze the function of $BaLi_4$ alloy sub-scaffold. After 10 mA h cm^{-2} Li was stripped, the internal porous array was further exposed, and the $BaLi_4$ microchannels array was evidenced as a secondary scaffold in the CC framework [Figure 2A]. As the Li stripping capacity reaches 20 mA h cm^{-2}, the ordered array of $BaLi_4$ alloy microchannels is uniformly dispersed on the carbon fibers, providing a large number of Li nucleation sites and facilitating Li ion diffusion [Supplementary Figure 5]. Furthermore, the lithiophilic Li-Ba alloy can reduce Li nucleation overpotential and inhibit Li dendrite generation during the subsequent process of Li plating. Therefore, when the Li is replated at 5 mA h cm^{-2} [Figure 2B], the plated Li preferentially fills the microchannels in

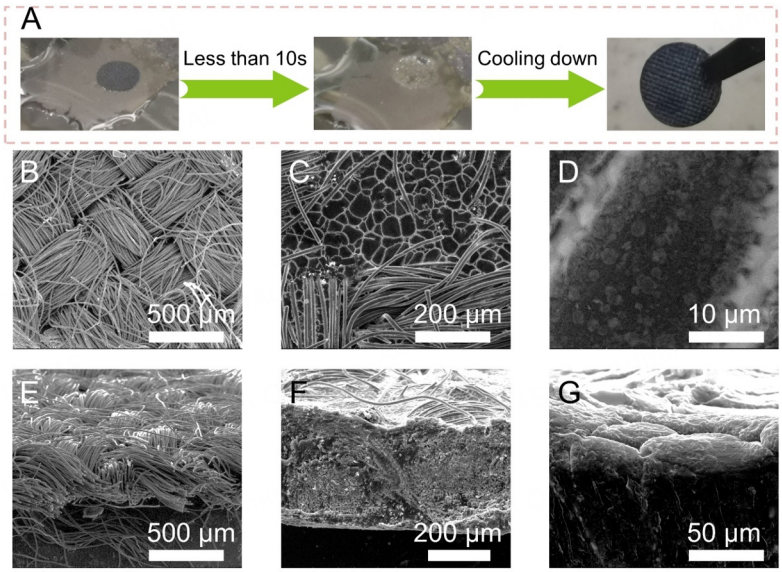

Figure 1. (A) Optical images of the liquid Li-Ba alloy infusion at 400 °C to CC. The top surface morphology of the (B) CC and the (C and D) LBAC electrodes. The cross-sectional view morphology of the (E) CC and the (F and G) LBAC.

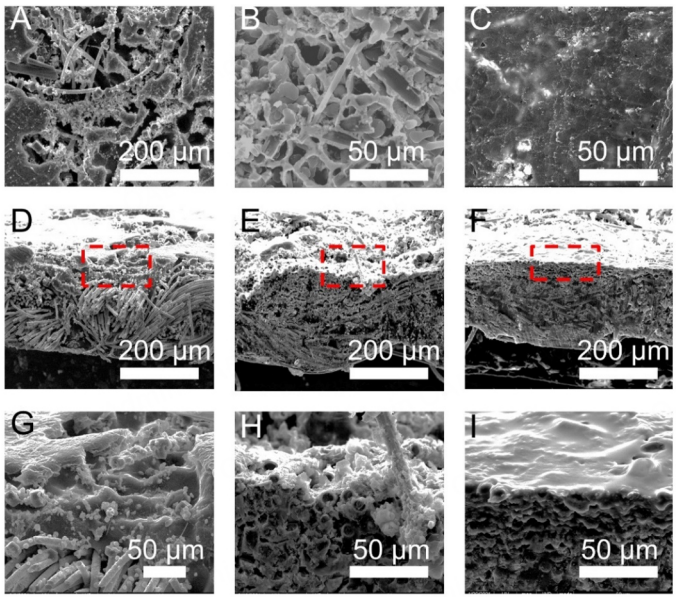

Figure 2. (A, D, G) The SEM images of LBAC anode following the removal of 10 mA h cm^{-2} Li, (B, E, H) subsequent deposition 5 mA h cm^{-2} and (C, F, I) 10 mA h cm^{-2} Li.

$BaLi_4$ alloy scaffold and no Li dendrite was visualized. The $BaLi_4$ microchannels can confine the deposited Li in a smaller cage, achieving uniform Li deposition behavior. As the Li plating capacity is up to 10 mA h cm^{-2}, the $BaLi_4$ microchannels are completely covered by Li metal, showing a dendrite-free morphology [Figure 2C]. Moreover, the dense Li layer can be observed in the side-view SEM images [Figure 2D-I]. These results demonstrate the significant impact of LBAC on guiding highly reversible Li stripping/plating behavior. This is attributed to the spatial confinement provided by porous $BaLi_4$ array among the bundles of carbon fibers, resulting in the reduced size of the deposited Li. In contrast, the Li-C electrode has a different Li stripping/plating behavior. A SEM image in Supplementary Figure 6A illustrates

that the Li metal in the vicinity of carbon fibers can be dissolved in a higher selectivity and increase the visibility of carbon fiber bundles, which may be attributed to the high electrical conductivity of the carbon fiber bundles. When replated with 5 mA h cm^{-2} Li [Supplementary Figure 6B], the severe aggregation of deposited Li metal on the upper surface of the CC is apparent clearly, indicating that the CC has a large Li nucleation overpotential which easily causes irregular Li deposition[57]. Notably, the deposited Li grows unrestrictedly since the Li deposition occurs on the upper surface. While the Li deposition capacity increases to 10 mA h cm^{-2}, the subsequently deposited Li metal accumulates on the previously deposited Li, causing the generation of numerous Li dendrites on the Li-C electrode [Supplementary Figure 6C-I]. This undesirable behavior poses a significant safety risk. These results clearly illustrate that the limited specific surface area and poor lithiophilicity of CC can result in uneven nucleation and unrestricted growth of Li to form Li dendrites.

To further evaluate the electrochemical performance for LBAC anodes, symmetrical cells were assembled using LBAC electrodes for assessing electrochemical cycling performances under different current densities. The Li-C/Li-C and Li-Ba/Li-Ba symmetric cells were also assembled separately for comparison to highlight the synergistic effect of the $BaLi_4$ alloy sub-framework and CC framework. As shown in Figure 3A, the time-voltage curve tells that the voltage hysteresis of LBAC cells can stabilize at 30 mV for 1,000 h under 1 mA cm^{-2}/1 mA h cm^{-2}, which is ascribed to the distinct multiscale scaffold structure of LBAC. By deep contrast, The Li-Ba symmetric cell has a much higher voltage hysteresis, especially after 200 h, demonstrating the aggregation of "dead Li" on the anode surface, leading to the cell failure. Similarly, the voltage polarization of Li-C cells increases abruptly at 350 h, which is much lower than that of the LBAC composite electrode. The lifespan of the Li-C and Li-Ba cells only maintains a shorter period with a larger overpotential after the current density exceeds 3 mA cm^{-2} (Li-Ba: ~120 mV for 140 h; Li-C: ~150 mV for 170 h). However, LBAC/LBAC cells exhibit longer cycling life without any voltage fluctuation (~40 mV for 420 h), which highlights the excellent Li affinity and structural stability of LBAC. The overpotential of LBAC anodes is much lower than Li-C anodes, which can be attributed to excellent lithiophilicity of Li-Ba alloy. Furthermore, the surface of LBAC anodes is not flat; in other words, the Li-rich Li-Ba alloy does not completely cover the CC surface, and the carbon fibers and Li-Ba alloy coexist on the LBAC anode surface. Therefore, LBAC anodes have larger specific area than Li-Ba anodes, exhibiting lower overpotential. The cells assembled with LBAC electrodes can cycle continuously for 220 h even at 5 mA cm^{-2}, while Li-Ba and Li-C-based cells can cycle for only 70 and 110 h with significant voltage fluctuations, separately. This can be attributed to the fact that the extremely high current density can trigger Li dendrite formation, while the interconnected microchannels in LBAC can confine the Li stripping/plating behavior in the alloy scaffold. Additionally, the larger specific surface area of LBAC anodes eliminates the high current density, so the Li dendrite growth can be effectively suppressed to ensure the cycling stability. As the typical areal capacity of commercially available Li-ion batteries is approximately 3 mA h cm^{-2}, the testing parameters are set to 3 mA/3 mA h cm^{-2}. Supplementary Figure 7 illustrates that the LBAC composite can achieve a cycling life of about 300 h. In contrast, the Li-Ba and Li-C cells display a short lifespan and the voltage hysteresis reaches 1,000 mV at 120 and 150 h due to the gradual thickening of the solid electrolyte interface (SEI) and the accumulation of inactive Li.

EIS were measured to assess the internal stability of symmetric cells, as shown in Figure 3B. The R_{ct} value of Li-Ba (~450 Ω) and Li-C symmetric cells (~550 Ω) is higher compared to LBAC symmetric cells before cycling (~200 Ω). After 100 cycles, the R_{ct} of the LBAC composite decreases to ~50 Ω, which remains smaller than that of the Li-Ba (75 Ω) and Li-C (125 Ω) cells, indicating that LBAC has faster charge transfer kinetics and a SEI layer with enhanced stability that facilitates reversible process of Li stripping/plating [Figure 3C]. The superior electrochemical performance indicates that the microchannels of the Li deposition behavior

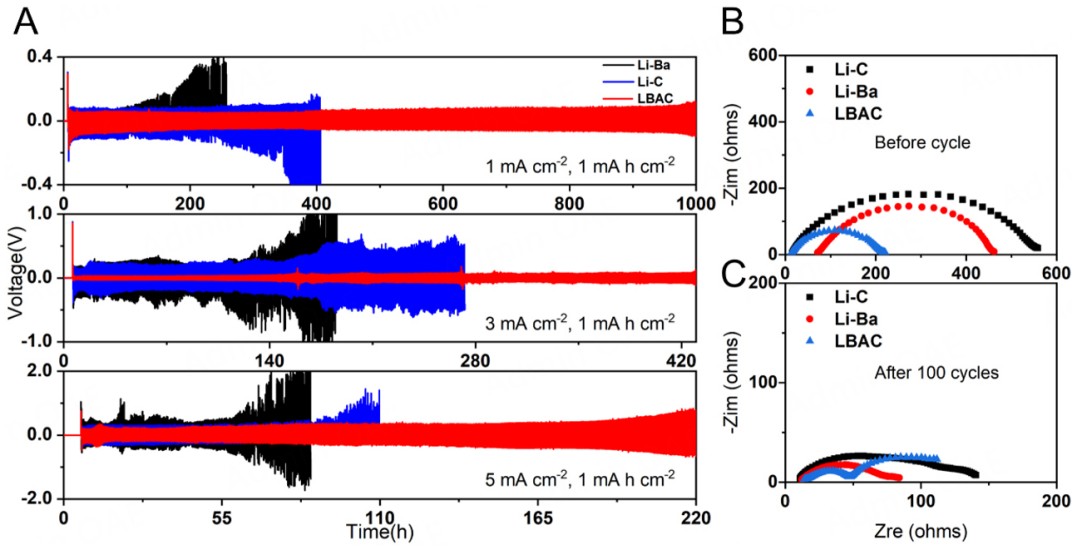

Figure 3. Electrochemical performances of LBAC, Li-Ba and Li-C symmetric cells at various current densities: (A) 1 mA cm^{-2}; 3 mA cm^{-2}; 5 mA cm^{-2}. Nyquist impedance plots of symmetrical cells with LBAC, Li-Ba and Li-C anodes (B) before and (C) after 100 cycles while operating at a condition of 3 mA cm^{-2}/1 mA h cm^{-2}.

can be effectively regulated by LBAC and the macroscopic skeleton of the CC enhances the stability of the multiscale scaffolds. Compared with the published records of the carbon-based Li composite anodes under the carbonate electrolyte conditions [Supplementary Table 2], the LBAC electrode exhibits superior cycling performance.

To acquire a profound comprehension of the function of LBAC on favorable long-term cycling lifespan, morphological evolution of LBAC and Li-C composite electrodes after 100 cycles is investigated, as depicted in Figure 4. After 100 cycles, a quantity of mossy and Li dendrites emerged on the Li-C surface, as illustrated in Figure 4A, delivering a rough and porous Li layer as thick as about 100 μm [Figure 4B and C]. The Li stripping/plating behavior in the LBAC electrode is well regulated by the $BaLi_4$ microchannels array. As shown in Figure 4D, the surface of the deposited Li is smooth, rather than showing Li dendrites, indicating that the favorable lithiophilicity and smaller pores of the $BaLi_4$ sub-scaffold can regulate uniform Li deposition. Figure 4E and F depicts no obvious "dead Li" and Li dendrites on the LABC top surface. Thus, the LBAC with microchannels array can effectively tune the Li growth process and ensure extraordinary cycling stability.

For evaluating the potential application of LBAC anodes in Li metal batteries, the full cells were assembled using LBAC as the anode and high-areal-capacity LFP as the cathode. Additionally, Li-C-based full cells were also assembled. The cycling performance is shown in Figure 5A. In initial cycles, a slight increase of specific capacity occurred in two cells due to the process of activating the electrode. The long-term cycling curve at 1 C demonstrates that the LBAC/LFP cell retains 93.3% of its initial capacity after 300 cycles (equal to 600 h), with a consistently stable coulombic efficiency (CE) of ~99.5%. On the contrary, the capacity retention of the Li-C/LFP full cell is significantly reduced (38.2%) and exhibits a sharp CE fluctuation even within 40 cycles, suffering from continuous capacity decay. Meanwhile, the rate performance was characterized by varying the current rate from 0.1 to 2 C. The LBAC/LFP cell can deliver specific capacities of 155 mA h g^{-1} (0.1 C), 147 mA h g^{-1} (0.5 C), and 135 mA h g^{-1} (1 C), exhibiting superior performance compared to the Li-C/LFP cells (0.1 C:154 mA h g^{-1}, 0.5 C:140 mA h g^{-1}, 1 C:119 mA h g^{-1}), as shown in Figure 5B-D. Even when the rate increases to 2 C (~4.9 mA cm^{-2}), the LBAC/LFP still gives a higher specific

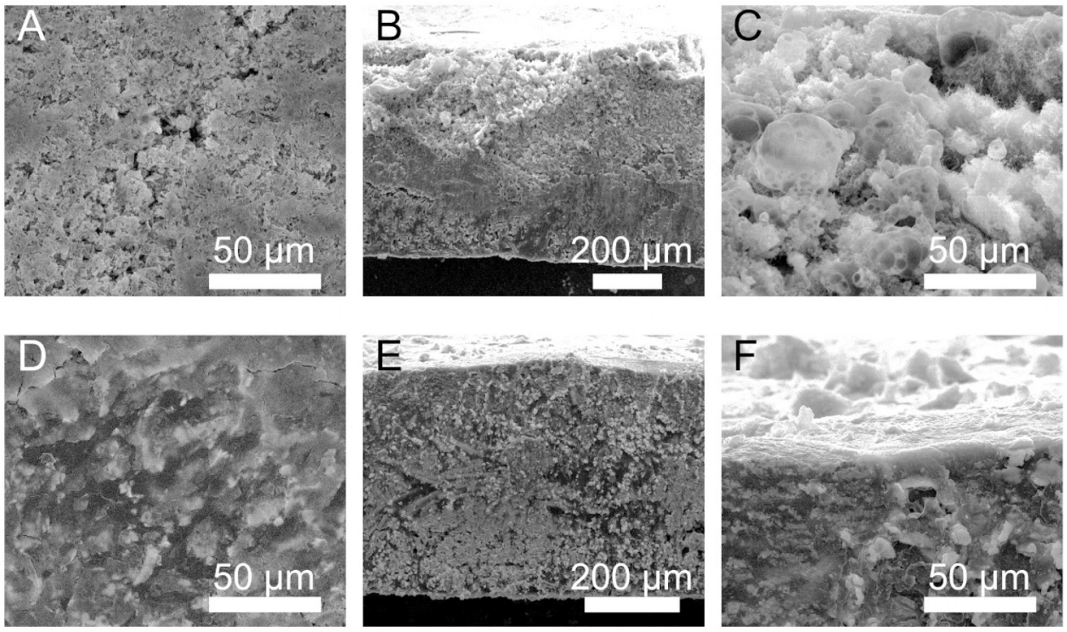

Figure 4. SEM images of (A-C) Li-C and (D-F) LBAC after 100 cycles. The cycling conditions are 3 mA cm^{-2} and 1 mA h cm^{-2}.

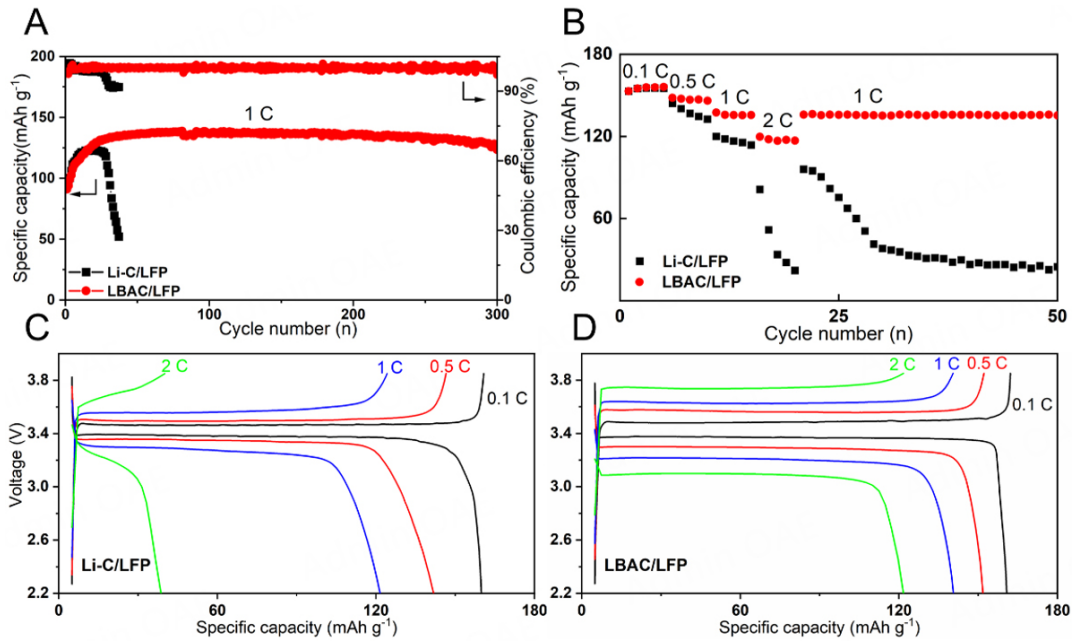

Figure 5. (A) The long-term electrochemical performance of the LBAC/LFP and Li-C/LFP full cells at 1 C. (B) Rate capability evaluation of the LBAC/LFP and Li-C/LFP from 0.1 to 2.0 C. Capacity-voltage curves of the (C) Li-C/LFP and (D) LBAC/LFP full cells as the anodes.

capacity of 117 mA h g^{-1}, with respect to 34 mA h g^{-1} of the Li-C/LFP cell. These results demonstrate that the lithiophilic $BaLi_4$ microchannel array as the sub-skeleton can significantly promote the rate performance and cyclic stability by effectively regulating Li deposition/dissolution behavior and suppressing Li dendrite growth.

CONCLUSIONS

In brief, we have successfully fabricated a remarkably stable Li composite anode with a porous $BaLi_4$ alloy array as the sub-skeleton in the CC sheet for regulating Li stripping/plating behavior via a facile thermal infusion strategy within 10 s. The addition of heteroatomic Ba metal to Li can reduce the surface tension of liquid Li, enhancing the wettability toward the CC. Moreover, the ordered array structure of LBAC anodes not only restricts the Li stripping/plating behavior in the microporous space to suppress Li dendrite growth but also reduces the Li nucleation overpotential to achieve homogeneous Li deposition. Furthermore, the mechanical strength of the anode is significantly enhanced by the excellent flexibility exhibited by the CC host. As a result, the porous array of $BaLi_4$ microchannels nested in CC sheet assists the high cycling performance over 1,000 h under a condition of 1 mA cm^{-2}/1 mA h cm^{-2} with a dendrite-free morphology. Additionally, a LBAC composite anode exhibits excellent performance in a full cell coupled with a LFP cathode due to the good reversibility and rapid transfer of charge. We believe a composite anode consisting of flexible carbon host architecture and Li-rich Li alloy with built-in lithiophilic and porous skeleton holds great potential as the practical anode material for Li metal batteries.

DECLARATIONS

Authors' contributions

Contributed substantially to conceptualization, investigation, formal analysis, and writing-original draft: Wang Z
Developed methodology: Chen T
Offered material support: Song Z, Xing J
Provided administration: Zhou A
Made significant contributions to project administration and technical review and editing: Li J

Availability of data and materials

Not applicable.

Financial support and sponsorship

This work was partly supported by the National Natural Science Foundation of China (Nos. 22379019 and 52172184), S&T Special Program of Huzhou (No. 2023GZ03), Huzhou Natural Science Foundation Project (Nos. 2022YZ04 and 2022YZ21), and National Science Foundation of Sichuan Province (No. 2022NSFSC0259).

Conflicts of interest

All authors declared that there are no conflicts of interest.

Ethical approval and consent to participate

Not applicable.

Consent for publication

Not applicable.

REFERENCES

1. Park S, Jin HJ, Yun YS. Advances in the design of 3D-structured electrode materials for lithium-metal anodes. *Adv Mater* 2020;32:2002193. DOI

2. Kang S, Cheng J, Gao W, Cui L. Toward safer lithium metal batteries: a review. *Energy Mater* 2023;3:300043. DOI
3. Ghazi ZA, Sun Z, Sun C, et al. Key aspects of lithium metal anodes for lithium metal batteries. *Small* 2019;15:e1900687. DOI
4. Zhang X, Yang Y, Zhou Z. Towards practical lithium-metal anodes. *Chem Soc Rev* 2020;49:3040-71. DOI
5. Jin C, Sheng O, Chen M, et al. Armed lithium metal anodes with functional skeletons. *Mater Today Nano* 2021;13:100103. DOI
6. Wang B, Xu T, Huang S, Kong D, Li X, Wang Y. Recent advances in carbon-shell-based nanostructures for advanced Li/Na metal batteries. *J Mater Chem A* 2021;9:6070-88. DOI
7. Wang C, Wang A, Ren L, et al. Controlling Li ion flux through materials innovation for dendrite-free lithium metal anodes. *Adv Funct Mater* 2019;29:1905940. DOI
8. Zhao Y, Ye Y, Wu F, Li Y, Li L, Chen R. Anode interface engineering and architecture design for high-performance lithium-sulfur batteries. *Adv Mater* 2019;31:e1806532. DOI
9. Peng HJ, Xu WT, Zhu L, et al. 3D carbonaceous current collectors: the origin of enhanced cycling stability for high-sulfur-loading lithium - sulfur batteries. *Adv Funct Mater* 2016;26:6351-8. DOI
10. Shi J, Nguyen HD, Chen Z, et al. Nanostructured block copolymer single-ion conductors for low-temperature, high-voltage and fast charging lithium-metal batteries. *Energy Mater* 2023;3:300036. DOI
11. Zhong Y, Cao C, Tadé MO, Shao Z. Ionically and electronically conductive phases in a composite anode for high-rate and stable lithium stripping and plating for solid-state lithium batteries. *ACS Appl Mater Interfaces* 2022;14:38786-94. DOI
12. Yue XY, Wang WW, Wang QC, et al. Cuprite-coated Cu foam skeleton host enabling lateral growth of lithium dendrites for advanced Li metal batteries. *Energy Stor Mater* 2019;21:180-9. DOI
13. Wang R, Shi F, He X, et al. Three-dimensional lithiophilic Cu@Sn nanocones for dendrite-free lithium metal anodes. *Sci China Mater* 2021;64:1087-94. DOI
14. Wang Z, Xue J, Liu Y, et al. Li_xCu alloy nanowires nested in Ni foam for highly stable Li metal composite anode. *Sci China Mater* 2022;65:69-77. DOI
15. Chi SS, Liu Y, Song WL, Fan LZ, Zhang Q. Prestoring lithium into stable 3D nickel foam host as dendrite-free lithium metal anode. *Adv Funct Mater* 2017;27:1700348. DOI
16. Eom JY, Choi SH, Kang JH, Eom GH, Moon J, Park MS. Rational design of a 3D Li-metal electrode for high-energy lithium batteries. *ACS Appl Energy Mater* 2021;4:1936-41. DOI
17. Jia W, Wang Y, Qu S, et al. ZnF_2 coated three dimensional Li-Ni composite anode for improved performance. *J Materiomics* 2019;5:176-84. DOI
18. Huang G, Chen S, Guo P, et al. In situ constructing lithiophilic NiF_x nanosheets on Ni foam current collector for stable lithium metal anode via a succinct fluorination strategy. *Chem Eng J* 2020;395:125122. DOI
19. Wang Q, Yang C, Yang J, et al. Stable Li metal anode with protected interface for high-performance Li metal batteries. *Energy Stor Mater* 2018;15:249-56. DOI
20. Li X, Yang G, Zhang S, Wang Z, Chen L. Improved lithium deposition on silver plated carbon fiber paper. *Nano Energy* 2019;66:104144. DOI
21. Xiao J, Xiao N, Liu C, et al. In situ growing chromium oxynitride nanoparticles on carbon nanofibers to stabilize lithium deposition for lithium metal anodes. *Small* 2020;16:2003827. DOI
22. Chen X, Lv Y, Shang M, Niu J. Ironing controllable lithium into lithiotropic carbon fiber fabric: a novel Li-metal anode with improved cyclability and dendrite suppression. *ACS Appl Mater Interfaces* 2019;11:21584-92. DOI PubMed
23. Jia W, Chen T, Wang Y, et al. Porous equipotential body with heterogeneous nucleation sites: a novel 3D composite current collector for lithium metal anode. *Electrochim Acta* 2019;309:460-8. DOI
24. Luo L, Li J, Yaghoobnejad Asl H, Manthiram A. A 3D lithiophilic Mo_2N-modified carbon nanofiber architecture for dendrite-free lithium-metal anodes in a full cell. *Adv Mater* 2019;31:e1904537. DOI
25. Wang Z, Deng Q, Song Z, et al. Ultrathin Li-rich Li-Cu alloy anode capped with lithiophilic LiC_6 headspace enabling stable cyclic performance. *J Colloid Interface Sci* 2023;643:205-13. DOI
26. Niu J, Yang J, Channa AI, et al. Enhancing the water splitting performance via decorating Co_3O_4 nanoarrays with ruthenium doping and phosphorization. *RSC Adv* 2020;10:27235-41. DOI PubMed PMC
27. Wang Y, Shen Y, Du Z, et al. A lithium-carbon nanotube composite for stable lithium anodes. *J Mater Chem A* 2017;5:23434-9. DOI
28. Zheng ZJ, Ye H, Guo ZP. Recent progress in designing stable composite lithium anodes with improved wettability. *Adv Sci* 2020;7:2002212. DOI PubMed PMC
29. Wang SH, Yue J, Dong W, et al. Tuning wettability of molten lithium via a chemical strategy for lithium metal anodes. *Nat Commun* 2019;10:4930. DOI PubMed PMC
30. Wang J, Wang H, Xie J, et al. Fundamental study on the wetting property of liquid lithium. *Energy Stor Mater* 2018;14:345-50. DOI
31. Shin HJ, Abbas S, Kim J, Cho J, Ha HY. Near-perfect suppression of Li dendrite growth by novel porous hollow carbon fibers embedded with ZnO nanoparticles as stable and efficient anode for Li metal batteries. *Chem Eng J* 2023;464:142713. DOI
32. Niu C, Pan H, Xu W, et al. Self-smoothing anode for achieving high-energy lithium metal batteries under realistic conditions. *Nat Nanotechnol* 2019;14:594-601. DOI
33. Zhu R, Yang H, Fadillah L, et al. A lithiophilic carbon scroll as a Li metal host with low tortuosity design and "Dead Li" self-cleaning capability. *J Mater Chem A* 2021;9:13332-43. DOI
34. Yue XY, Li XL, Wang WW, et al. Wettable carbon felt framework for high loading Li-metal composite anode. *Nano Energy*

2019;60:257-66. DOI
35. Wang L, Zhu X, Guan Y, et al. ZnO/carbon framework derived from metal-organic frameworks as a stable host for lithium metal anodes. *Energy Stor Mater* 2018;11:191-6. DOI
36. Le T, Yang C, Liang Q, Huang X, Kang F, Yang Y. A fishing-net-like 3D host for robust and ultrahigh-rate lithium metal anodes. *Small* 2021;17:e2007231. DOI
37. Chen XR, Li BQ, Zhu C, et al. A coaxial-interweaved hybrid lithium metal anode for long-lifespan lithium metal batteries. *Adv Energy Mater* 2019;9:1901932. DOI
38. Deng W, Zhu W, Zhou X, Peng X, Liu Z. Highly reversible Li plating confined in three-dimensional interconnected microchannels toward high-rate and stable metallic lithium anodes. *ACS Appl Mater Interfaces* 2018;10:20387-95. DOI
39. Cao J, Xie Y, Li W, et al. Rationally optimized carbon fiber cloth as lithiophilic host for highly stable Li metal anodes. *Mater Today Energy* 2021;20:100663. DOI
40. Gong YJ, Pyo S, Kim H, et al. Advanced Li metal anode by fluorinated metathesis on conjugated carbon networks. *Energy Environ Sci* 2021;14:940-54. DOI
41. Wang X, Pan Z, Wu Y, et al. Infiltrating lithium into carbon cloth decorated with zinc oxide arrays for dendrite-free lithium metal anode. *Nano Res* 2019;12:525-9. DOI
42. Zhang P, Peng C, Liu X, et al. 3D lithiophilic "Hairy" Si nanowire arrays @ carbon scaffold favor a flexible and stable lithium composite anode. *ACS Appl Mater Interfaces* 2019;11:44325-32. DOI
43. Zhang YJ, Liu SF, Wang XL, et al. Composite Li metal anode with vertical graphene host for high performance Li-S batteries. *J Power Sources* 2018;374:205-10. DOI
44. Liu T, Hu J, Li C, Wang Y. Unusual conformal Li plating on alloyable nanofiber frameworks to enable dendrite suppression of Li metal anode. *ACS Appl Energy Mater* 2019;2:4379-88. DOI
45. Zhang R, Chen X, Shen X, et al. Coralloid carbon fiber-based composite lithium anode for robust lithium metal batteries. *Joule* 2018;2:764-77. DOI
46. Go W, Kim MH, Park J, et al. Nanocrevasse-rich carbon fibers for stable lithium and sodium metal anodes. *Nano Lett* 2019;19:1504-11. DOI
47. Feng YQ, Zheng ZJ, Wang CY, et al. A super-lithiophilic nanocrystallization strategy for stable lithium metal anodes. *Nano Energy* 2020;73:104731. DOI
48. Fang Y, Zhang Y, Zhu K, et al. Lithiophilic three-dimensional porous $Ti_3C_2T_x$-rGO membrane as a stable scaffold for safe alkali metal (Li or Na) anodes. *ACS Nano* 2019;13:14319-28. DOI
49. Liu S, Xia X, Zhong Y, et al. 3D TiC/C core/shell nanowire skeleton for dendrite-free and long-life lithium metal anode. *Adv Energy Mater* 2018;8:1702322. DOI
50. Kwon H, Lee JH, Roh Y, et al. An electron-deficient carbon current collector for anode-free Li-metal batteries. *Nat Commun* 2021;12:5537. DOI PubMed PMC
51. Patrike A, Suresh K, Wahid M, Chaturvedi V, Shelke MV. Ice-colloidal templated carbon host for highly efficient, dendrite free Li metal anode. *Carbon* 2021;179:256-65. DOI
52. Pathak R, Chen K, Wu F, et al. Advanced strategies for the development of porous carbon as a Li host/current collector for lithium metal batteries. *Energy Stor Mater* 2021;41:448-65. DOI
53. Wang C, Xie H, Zhang L, et al. Universal soldering of lithium and sodium alloys on various substrates for batteries. *Adv Energy Mater* 2018;8:1701963. DOI
54. Yang C, Xie H, Ping W, et al. An electron/ion dual-conductive alloy framework for high-rate and high-capacity solid-state lithium-metal batteries. *Adv Mater* 2019;31:e1804815. DOI
55. Jia W, Wang Z, Li J, et al. A dual-phase Li-Ca alloy with a patternable and lithiophilic 3D framework for improving lithium anode performance. *J Mater Chem A* 2019;7:22377-84. DOI
56. Jia W, Chen J, Wang Z, Zhou A, Hu YS, Li J. Dendrite-free dual-phase Li-Ba alloy anode enabled by ordered array of built-in mixed conducting microchannels. *Small* 2023;20:2308279. DOI PubMed
57. Wang Z, Liu Y, Xing J, et al. Li-Ca Alloy composite anode with ant-nest-like lithiophilic channels in carbon cloth enabling high-performance Li metal batteries. *Research* 2022;2022:9843093. DOI